0031-3998/10/6801-0023
PEDIATRIC RESEARCH

Vol. 68, No. 1, 2010
Printed in U.S.A.

Gastroschisis in Mice Lacking Aortic Carboxypeptidase-Like Protein Is Associated With a Defect in Neuromuscular Development of the Eviscerated Intestine

ENRICO DANZER, MATTHEW D. LAYNE, FREDERIC AUBER, SHINCY SHEGU, PORTIA KREIGER, ANTONETA RADU, MARYANN VOLPE, N. SCOTT ADZICK, AND ALAN W. FLAKE

The Center for Fetal Research [E.D., F.A., S.S., P.K., A.R., N.S.A., A.W.F.], Children's Hospital of Philadelphia, University of Pennsylvania School of Medicine, Philadelphia, Pennsylvania 19104; Department of Biochemistry [M.D.L.], Boston University School of Medicine, Boston, Massachusetts 02118; Department of Pediatrics [M.A.V.], Floating Hospital for Children, Tufts Medical Center, Tufts University School of Medicine, Boston, Massachusetts 02111

ABSTRACT: Mice lacking aortic carboxypeptidase-like protein (ACLP) exhibit a gastroschisis (GS) like abdominal wall defect. The objectives of this study were to evaluate the pathophysiological features of GS in ACLP$^{-/-}$ mice and to characterize the neuromuscular development of the eviscerated intestine (EI). ACLP$^{-/-}$ mice were created by heterozygous mating from previously generated mice with targeted disruption of ACLP. Specimens were processed for H&E, and immunohistochemistry for smooth muscle cells [SMC, α-smooth muscle actin (α-SMA) antibody], interstitial cells of Cajal (ICC, c-kit-antibody), neural crest cells (NCC, Hox-b5-antibody), and enteric neurons (EN, PGP9.5-, α-internexin, and synaptophysin antibody). From 47 fetuses genotyped, 13 (27.7%) were wild type, 20 (42.5%) were heterozygous, and 14 (29.8%) were ACLP homozygous. In GS mice, expression of c-kit, Hox-b5, PGP-9.5, α-internexin, and synaptophysin were almost completely absent and only faint α-SMA expression was seen in the EI. In contrast, c-kit, Hox-b5, PGP9.5, α-internexin, synaptophysin, and α-SMA expression in intra-abdominal intestine in GS fetuses was the same as control intestine. The defect observed in ACLP$^{-/-}$ mice closely resembles GS. Absence of ICC, NCC, EN, and immature differentiation of SMC supports an associated defect in neuromuscular development that is restricted to the EI. **(*Pediatr Res* 68: 23–28, 2010)**

Gastroschisis (GS) is a relatively common congenital malformation characterized by evisceration of fetal intestine into the amniotic fluid (AF) through an abdominal wall defect (AWD) adjacent to the umbilicus. Eviscerated loops are shortened and may be covered by an inflammatory fibrin peel. Clinically, GS is associated with a broad spectrum of gastrointestinal (GI) complications ranging from mechanical issues of intestinal atresia to functional issues of dysmotility and malabsorption resulting in feeding intolerance (1). Significant morbidity occurs in infants with prolonged feeding intolerance related to complications of parenteral nutrition (*i.e.* sepsis and liver failure). Particularly problematic are a subset of GS patients that experience ongoing feeding problems throughout life (2).

In an effort to understand the mechanism of GS induced intestinal damage, surgically created animal models have been developed (3,4). However, the relevance of surgically created models to GS can be questioned because of the relatively late timing of creation of the AWD and the potential for surgically induced artifact. Genetic models of AWDs have also been described (5–8). Unfortunately, most genetic models exhibit additional abnormalities not seen in GS and may therefore not be comparable to GS. Thus far, an ideal model of GS that is naturally occurring, and mimics the developmental aspects and pathophysiology of GS has not yet been identified.

A genetic model of mice lacking aortic carboxypeptidase-like protein (ACLP) that exhibit a GS-like AWD has been recently described by one of the authors (M.D.L.) (9). ACLP is a member of a diverse group of proteins that contains a signal peptide at the N-terminus, an extensin domain, a discoidin domain, and a catalytically inactive metallocarboxypeptidase domain at its carboxyl terminus (9). During embryonic development, ACLP is highly expressed in vascular smooth muscle cells (SMC), within the abdominal wall, in the dermal layer of the skin, and the developing skeleton (10). This study was designed to evaluate the pathophysiological features of GS in ACLP$^{-/-}$ mice and to investigate the neuromuscular development of the eviscerated intestine (EI). Our findings identify profound alterations in neuromuscular development that are limited to the EI.

MATERIALS AND METHODS

All experimental protocols were approved by the Institutional Animal Care and Use Committee at The Children's Hospital of Philadelphia and Harvard Medical Area Standing Committee on Animals Boston and followed guidelines set forth in the National Institutes of Health Guide for Care and Use of Laboratory Animals.

Animals. ACLP$^{-/-}$ mice were generated as previously described (9). Timed pregnant mice were anesthetized by isoflurane and euthanized by cervical dislocation near term (E18.5). Fetuses were delivered by cesarean section under a dissecting microscope. Body wall morphology was examined and photographed, and the fetuses were placed on ice. Body weight and length

Received October 8, 2009; accepted March 29, 2010.
Correspondence: Alan W. Flake, M.D., The Children's Hospital of Philadelphia, The Center for Fetal Research, Abramson Research Center, Rm. 1116, 3615 Civic Center Blvd., Philadelphia, PA 19104-4318; e-mail: flake@email.chop.edu

Abbreviations: AWD, abdominal wall defect; **ACLP,** aortic carboxypeptidase-like protein; **EI,** eviscerated intestine; **GS,** gastroschisis; **ICC,** interstitial cells of Cajal; **NCC,** neural crest cells; **SMC,** smooth muscle cells; **TIWT,** total intestinal wall thickness; **VH,** villus height; **VW,** villus width

were recorded. Mice were genotyped by genomic Southern blot analysis of DNA isolated from tail biopsies extracted as described elsewhere (9). In randomly selected GS and non-GS fetuses the intestine was removed from the pylorus to the rectum. The removed intestine was weighed and its length was measured to calculate the intestinal weight per unit length.

General morphology and immunohistochemistry. After fixation in 10% neutral buffered formalin (Sigma Chemical Co.), fetuses assigned for immunohistochemical analyses were dehydrated in alcohol, paraffin embedded and sectioned (4 μm). For general morphology, sections were deparaffinized, rehydrated to distilled water, and stained with H&E or Masson's Trichrome according to standard protocols. Immunohistochemical techniques for light and immunofluoresence microscopy were performed as described previously (11). The following primary antibodies were used: mouse anti-alpha-smooth muscle actin (α-SMA; DAKO Cytomation, Glostrup, Denmark, 1:100), rabbit anti-c-kit (CD 117; DAKO Cytomation, Glostrup, Denmark, 1:25), rabbit anti-Hoxb5 (Dr. MaryAnn Volpe, Tufts Medical Center, Boston, MA, 1:200), rabbit antiprotein gene product 9.5 protein (PGP9.5; Abcam Inc, Cambridge, MA, 1:200), rabbit anti-synaptophysin (DakoCytomation, Glostrup, Denmark, 1:100), and rabbit anti-alpha internexin (Abcam Inc, Cambridge, MA, 1:100).

Morphologic analysis. H&E-stained sections were used to measure total intestinal wall thickness (TIWT), villus height (VH), and villus width (VW). TIWT was blindly examined with a light microscope (Axioimager AX10, Carl Zeiss, Germany) interfaced with a digital camera (Axiocam HRc, Carl Zeiss, Germany) connected to a PC computer (Antec Aria, Fremont, CA). Digital images were acquired (400× final magnification) and analyzed using Axiovision 4.5 software (Carl Zeiss, Germany). At least 10 TIWT measurements were taken and averaged. VH and VW were analyzed as previously described using the same image analysis system (12). At least 20 villi were counted and averaged. Only villi in which the central lymphatic channel could be visualized were measured. Finally, villus density was determined by counting all villus visible cross-sections.

Quantitative analysis of interstitial cells of Cajal and NCC. The density of distribution of c-kit positive interstitial cells of Cajal (ICC) was graded after evaluation of five well stained and well oriented high-power fields (400× final magnification, Axioimager AX10, Carl Zeiss, Germany) with the field having an area of 0.0891 mm^2. The grades sparse, few, moderate, and many reflected an average count of 0–2, 3–7, 8–12, and >12 cell bodies per high-power field, respectively (13). Only ICC's with nuclei were counted. Quantitative analysis of hoxb5-positive neural crest cells (NCC) was performed according to previously described methods (14). Briefly, NCC were counted and quantified as the number of cells per high-power visual field (400×, Axioimager AX10, Carl Zeiss, Germany, area of 0.0891 mm^2). Five randomly chosen fields per eviscerated and non-EI per animal (n = 6 for GS fetuses and controls) were analyzed. The observer was blinded to animal identification (S.S.).

Statistical analysis. Numerical data are presented as mean ± SD. Statistical differences were identified using one-way ANOVA, χ^2, or Fisher Exact tests with posthoc testing where appropriate. All statistical tests were performed using JMP statistical software package (V 7.0, SAS Corp, Cary, NC). A p value of less than 0.05 was considered statistically significant.

RESULTS

Characterization of ACLP mice. ACLP± mice were phenotypically normal (9). The genotype distribution of fetuses (n = 47) obtained from ACLP heterozygous mating in this study were 13 (28%) ACLP$^{+/+}$, 20 (42%) ACLP±, and 14 (30%) ACLP$^{-/-}$. As no anatomical differences between wild-type and heterozygous ACLP mice exists, (9) ACLP$^{+/+}$ and ACLP ± mice were grouped together as control group.

All mice lacking ACLP exhibited GS (Fig. 1*A-E*) characterized by evisceration of fetal intestine into the AF through an AWD adjacent to the umbilicus. On gross examination, EI appeared dilated, but in contrast to some human infants (Fig. 1*F*), peel formation or adhesions between loops were not observed. GS mice appeared normal in size and fetuses analyzed at E18.5 were equivalent in birth weight (controls: 1.2 ± 0.2 g *versus* GS: 1.1 ± 0.2 g; p = 0.2) and crown-rump length (controls: 22.6 ± 1.9 mm *versus* GS: 21.9 ± 2.4 mm; p = 0.4) compared with control littermates. Intestinal length (controls: 10.2 ± 0.8 cm *versus* GS: 10.3 ± 0.6 cm; p = 0.8) and intestinal weight per unit length (controls: 11.5 ± 0.9 mg/cm *versus* GS: 11.7 ± 0.7 mg/cm; p = 0.3) were similar between groups. No morphologic abnormalities of the ventral wall, with the exception of the GS defect, were seen in GS mice compared with controls.

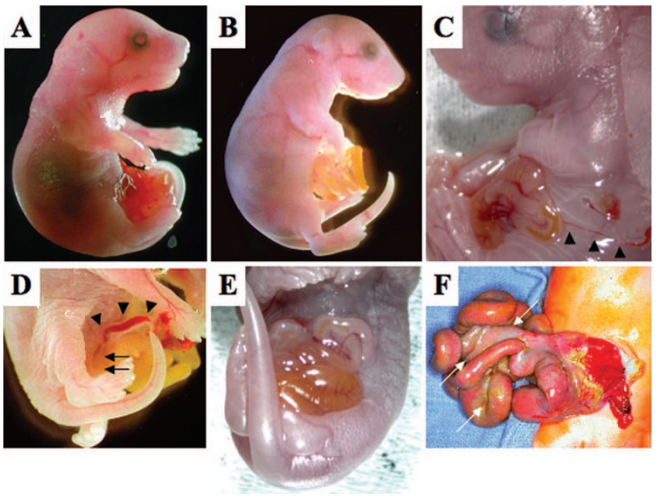

Figure 1. GS in ACLP$^{-/-}$ fetuses. *A-E*, Representative photomicrographs of term fetuses (E18.5). *C*, The umbilical cord is found to the left of the defect. The umbilical artery is filled with blood (*black arrowheads*). *D*, Evisceration of fetal intestine through an AWD adjacent to the umbilicus, black arrowheads point toward the umbilical artery and black arrows toward the AWD. *F*, Representative photomicrograph of a newborn with GS. Compared with humans, where the eviscerated intestinal loops are shortened, matted, and covered by a fibrous peel (*white arrows*); the EI in ACLP$^{-/-}$ mice lacks these pathologic changes.

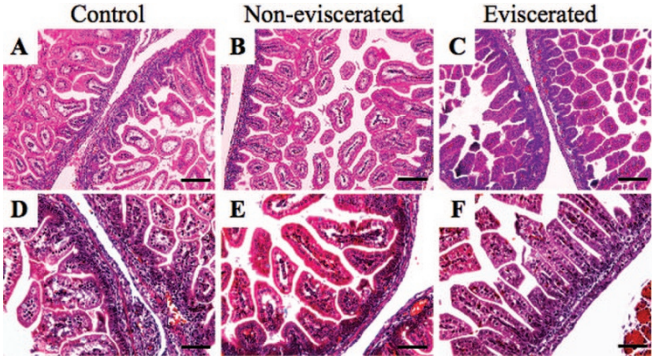

Figure 2. Histologic presentation of the intestinal morphology at E18. *A-C*, H&E stained section of the fetal intestine. Note the absence of peel formation in the EI. *D-F*, Cross-section stained with Masson's trichrome. No increase in extracellular matrix protein deposition was observed. Original magnification 100× (*A-F*).

Intestinal morphology. Bowel wall thickening or peel formation were not observed in the EI (Fig. 2). Mean TIWT was not significantly different between groups (control TIWT: 57.1 ± 6.9 μm, noneviscerated TIWT: 55.8 ± 8.4 μm, eviscerated TIWT: 56.6 ± 14.2 μm; p = 0.42). Compared with controls, mean VH and VW of the EI in ACLP$^{-/-}$ mice with GS was significantly reduced (control VH: 160.7 ± 29.5 μm, noneviscerated VH: 169.1 ± 40.8 μm, eviscerated VH: 136.5 ± 26.8 μm; p = 0.02; control VW: 56.4 ± 6.4 μm, noneviscerated VW: 64.1 ± 9.8 μm, eviscerated VW: 49.2 ± 10.2 μm; p = 0.02).

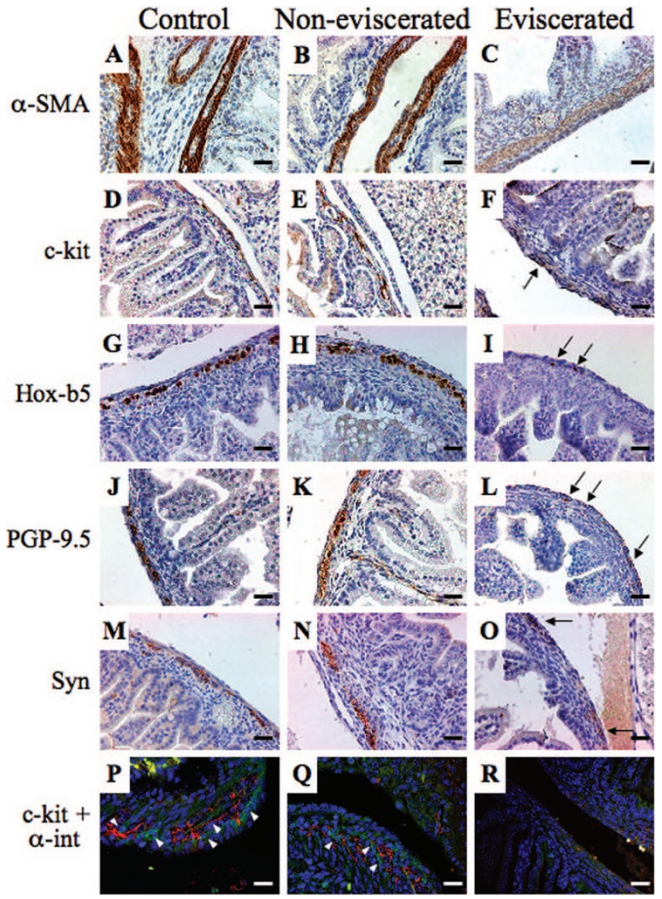

Figure 3. Immunohistochemical evaluation of the fetal intestine at E18. (α-SMA). Although no differences in staining intensity were found in control intestine (*A*) and the intestine of GS mice that remained inside the abdominal cavity (*B*); the EI (*C*) showed only a faint, immature expression of α-SMA within the circular muscle layer only. (c-kit). Spindle-shaped c-kit positive ICC is evenly distributed within the tunica muscularis in control (*D*) specimen and non-EI of GS mice (*E*). However, in the EI (*F*) there is an almost complete absence of ICC (*arrow*). (Hox-b5). No difference in the expression pattern of Hox-b5 positive NCC inside the abdominal wall between control (*G*) and mice with GS (*H*). However, Hox-b5 positive NCC (*black arrow*) could rarely be found in the EI (*I*). (PGP9.5 and synaptophysin). PGP-9.5 positive enteric neurons and synaptophysin positive nerve varicosities were found clustered into ganglia throughout the myenteric plexuses of the intestinal wall in control intestine (*J* and *M*) and non-EI (*K* and *N*). In contrast, within the EI (*L* and *O*), PGP9.5 positive enteric neurons, and synaptophysin positive nerve varicosities could rarely be observed (*arrows*). (Double-immunostaining c-kit/α-internexin). c-kit positive ICC (*green*) and α-internexin (*red*) positive enteric nerve fibers form a strong network (*arrowheads*) within the tunica muscularis in controls (*P*) and intestine from GS-mice that remains inside the abdominal cavity (*Q*). This close association between ICC and neural elements is necessary to mediate enteric motor neurotransmission and coordinated excitability of smooth muscle within the intestinal wall. This dense network however, is completely absent in the EI (*R*). Original magnification 200×, (*A-R*).

Smooth muscle cell development. The staining pattern for the non-EI was similar to that of control tissue (Fig. 3*A* and *B*). We observed an intense immunoreactivity for α-SMA and the outer longitudinal and inner circular muscle layer are easily distinguishable, indicating that normal development and differentiation of the SMC within the control intestine has occurred. Within the EI however, staining intensity was not only weaker than that of controls; we observed only one discrete band of α-SMA immunoreactivity (Fig. 3*C*).

Table 1. *Density scores for ICC distribution in control, noneviscerated, and eviscerated ACLP intestine*

	Control intestine (%)	Non-eviscerated intestine (%)	Eviscerated intestine (%)
Sparse	3	4	49*
Few	15	14	28*
Moderate	56	43	20*
Many	26	39	3*

The grades sparse, few, moderate, and many reflected an average count of 0–2, 3–7, 8–12, and >12 cell bodies per high-power field (400×), respectively. Data presented as %.

* Chi-square distribution analysis revealed significant differences in density of ICC between controls (control intestine and non-eviscerated intestine) and eviscerated intestine, $p < 0.001$.

Interstitial cells of Cajal. In control, intestine numerous ICC were readily discernable throughout the intestinal wall (Fig. 3*D* and *E*). The c-kit immunoreactive cells were situated within the circular and longitudinal muscle layer running parallel to the long axis of the muscle fibers. Morphologically, the ICC's were small, fusiform cells with two, occasional three extensions, had an ovoid nucleus and formed an intensive network within the intramuscular space. In contrast to controls, the density and distribution of ICC within the EI in GS were profoundly altered. Morphologically, c-kit immunoreactive cells lost their typically spindle shaped appearance. Moreover, ICC's were nearly nonexistent and individual ICC failed to form a continuous network between the circular and the longitudinal muscle layers (Fig. 3*F*). This observation was confirmed by quantitative analysis. Although no statistical difference was found in the density of ICC between control and non-EI ($p = 0.2$), density scores were significantly reduced in the EI compared with controls ($p < 0.001$) (Table 1).

Enteric NCC. As shown in Figure 3*G*, intense Hox-b5 immunoreactivity of the enteric neuronal precursors, grouped within well-defined myenteric plexuses was observed in normal intestinal specimens and the non-EI of GS mice. Analysis of the eviscerated intestine, however, showed significant differences in distribution pattern of Hox-b5 immunoreactive enteric NCC compared with controls. Only a few scattered Hox-b5 positive neuroblasts were encountered (Fig. 3*I*). Occasional aggregates of enteric NCC were seen within the developing myenteric plexuses, but in the most damaged EI Hox-b5 immunoreactive neuroblasts were completely absent. Quantitatively, we observed a significant reduction ($p < 0.001$) of NCC within the EI from GS mice (9.4 ± 7.5) compared with controls (93.3 ± 24.7) and non-EI (93.8 ± 18.9). To determine, whether GS is associated with a migration abnormality of the NCC we analyzed the hindgut (*i.e.* colon, rectum) in ACLP$^{-/-}$ mice. No differences in the spatial arrangement of Hox-b5 immunoreactive NCC were found between groups (data not shown).

Enteric nerves, ganglion, and synaptic activity. PGP9.5 immunoreactivity of the control intestine showed prominent enteric neurons within the myenteric ganglia, and darkly stained axons within the SMC layers (Fig. 3*J*). Intensive PGP9.5 labeling was seen in the nerve strands and cell pro-

cesses connecting myenteric ganglia. A moderate supply of positive fibers was detected in the muscularis mucosa and the villous lamina propria. Likewise, similar PGP9.5 immunoreactive specificity and distribution pattern were identified in the non-EI of ACLP$^{-/-}$ mice with GS (Fig. 3*K*). In the EI, PGP9.5 was detected only in small, faintly labeled neurons (Fig. 3*L*), which were only occasionally found to form mature ganglia. Furthermore, positive nerve fibers were no longer demonstrable between individual myenteric ganglia plexuses. Cell-specific synaptophysin immunoreactivity localized to nerve varicosities within the longitudinal and circular muscle layer were observed in control intestine (Fig. 3*M* and *N*). However, only minimal immunoreactive varicosities that were rarely grouped were found within the EI (Fig. 3*O*).

Relationship between enteric nerves and ICC. To determine whether the relationship between enteric nervous system (ENS) and ICC is abnormal in the eviscerated intestine, double immunohistochemical experiments using antibodies to α-internexin and c-kit were performed. In the control (Fig. 3*P*) and noneviscerated (Fig. 3*Q*) intestine, double-immunolabeling revealed a dense network of ICC that was closely apposed to neural elements within the circular and longitudinal muscle layers. However, this dense network between ICC and enteric neurons was completely absent in the EI (Fig. 3*R*).

DISCUSSION

Over the past 20 y, there has been an increase in the incidence of GS worldwide. Although overall survival for newborns with GS is good, these infants often suffer from prolonged intestinal dysmotility with associated malabsorption, failure to thrive, and prolonged total parenteral nutritional support (1,2). Prevention of these complications requires an understanding of the underlying pathophysiologic mechanisms. Recently, Layne *et al.* (9) observed that mice lacking ACLP display an AWD that seems similar to GS. Subsequently, the gene encoding ACLP has been co-localized with the quantitative trait locus for radiation-induced GS on chromosome 11, (15) suggesting that ACLP may indeed be involved in the development of GS. These findings combined with the limitations of the current animal models prompted our analysis of the gross morphologic and histopathological features of the ACLP$^{-/-}$ mice to clarify whether the ACLP mouse model could potentially be an appropriate model for future experimental studies of GS.

We found that ACLP$^{-/-}$ mice recapitulate many characteristics of GS. All homozygous ACLP$^{-/-}$ fetuses in this study developed persistent intestinal herniation through an AWD adjacent to the umbilicus. Unlike other genetic models that display GS as part of a maldevelopment of the entire ventral body wall, evisceration of intestine in the ACLP$^{-/-}$ fetuses appears anatomically similar to human GS. Furthermore, nonGS related malformations were not found in homozygous fetuses when examined by microscopic techniques. This represents an important advantage of the ACLP model as the presence of associated malformations in other genetic models of GS raises questions about the relevance of the defect to human GS and has the potential to confound the analysis (5–8). Of note, in contrast to human GS where the AWD is almost always on the right side of the umbilicus, the AWD in ACLP$^{-/-}$ fetuses is more closely related to the midline of the abdominal wall. As the embryonic events that result in GS have been the source of speculation and controversy, further analysis of the abdominal wall closure in the ACLP mouse model may help to further elucidate the mechanisms involved in body wall closure and the development of persistent evisceration of fetal intestine during early embryogenesis.

As the etiology of the intestinal dysmotility in GS has yet to be clarified, the primary aim of our study was to evaluate neuromuscular development of the EI in ACLP$^{-/-}$ mice using morphologic and immunohistochemical techniques. We did not observe fibrous peel formation, bowel adherence, or shortening of the overall intestinal length. Althoughs these results contrast with the observation of pronounced peel development on the serosal surface in some surgical created models (3,4), our data are in accordance with recent clinical studies that also reported absence of fibrous peel in many human fetuses and newborns with GS (16–18). In an elegant series of morphologic studies on intestinal specimens obtained from human GS fetuses between 10 and 40 wk gestation, Tibboel *et al.* (18) demonstrated that the development of fibrotic peel occurs late in gestation (3rd trimester). Subsequent studies showed that GS infants that were delivered prematurely (<36 wk) often have less peel formation than full-term GS newborns (16,17), supporting the hypothesis that peel development occurs predominantly in the last weeks of gestation. Hence, the absence of peel formation in the ACLP$^{-/-}$ mice might be explained by the relatively short gestation of the ACLP model.

On the basis of our hypothesis that the observed GI dysmotility in GS could be related to an abnormal neuromuscular development of the EI, we used a panel of immunohistochemical markers to study SMC, ICC, NCC, and enteric neurons. SMC play a pivotal role in the intestinal peristalsis. It is known that the intestinal musculature develops sequentially beginning in the circular layer, followed by the longitudinal layer, and finally within the muscularis mucosa (19). We found a major difference in the extent of SMC development and maturation between controls and the EI. Although in the non-EI of ACLP$^{-/-}$ mice and controls the SMC were strongly positive and outer longitudinal and inner circular muscle layers were easily discernable, the SMC within the EI were faintly immunoreactive and instead of two layers only one distinct layer of SMC was formed suggesting that the development of the longitudinal muscle layer within the EI might be delayed. This assertion is supported by our previous studies in the surgical created GS rat model, where we demonstrated that SMC differentiation of the eviscerated fetal rat intestine at term (E22) mimics the immature pattern of E18 control intestine (20).

It has been widely accepted that ICC are of fundamental importance in regulating GI motility and enteric motor neurotransmission (21,22). Under normal conditions, ICC form an uninterrupted network along the digestive tract and the lack of ICC in a segment of the GI tract can induce a local motility disturbance (22). We found a significant diminution of c-kit staining within the EI in homozygous ACLP mice, suggesting

that exposure of the fetal intestine to the AF subsequently results in a loss of ICC. Our data are in agreement with a recent study by Midrio *et al.*, (20) who demonstrated an abnormal development of ICC within the EI in a surgical created model. On the basis of these results, it is tempting to speculate that the relative absence of ICC's within the EI may represent an underlying morphologic cause for the decreased smooth muscle contractile activity, thereby contributing to the observed GI dysmotility in GS.

Another important aspect in the pathophysiology of intestinal dysmotility in GS is the loss of enteric neural elements. First, we used Hoxb5 a NCC marker (23). Our results suggest that, exposure to the AF results in a significant reduction of hoxb5 positive NCC within the EI. Subsequently, we used several immunohistochemical markers that are expressed by enteric neurons: PGP-9.5, synaptophysin, and α-internexin (24–26). We found a profound gradient of PGP-9.5, synaptophysin, and α-internexin immunoreactive enteric ganglia between the eviscerated and noneviscerated intestine. Our data demonstrate that GS is not only associated with a decreased distribution of enteric neurons but also associated with an abnormal cytoskeletal organization and reduced synaptic activity within the EI. Consequently, it is possible to conclude that the lack or reduction of normal ENS maturation subsequently impairs normal peristalsis. Whether the observed abnormal development of the ENS might be, at least in part, caused by exposure to the AF is currently unknown. However, previous data obtained from surgical created GS models in which the artificial exposure of the fetal bowel also demonstrated a significant disturbance of ENS organization and maturation (27,28). Future studies however are required to reveal the specific cellular mechanisms that are accountable for the observed morphologic changes of the ENS in the EI.

Despite our intriguing data, the limitations of our study should be acknowledged. Our data are based on histomorphological assessment, thus we can only speculate on the functional significance of our findings. Combining the structural results with functional analysis would allow us to evaluate the impact of the abnormal neuromuscular development of the EI on the overall GI dysmotility. However, because of the fragility of the fetal mouse intestine at term (E18.5) contractility studies could not be performed. In addition, because of the relatively short gestation age of the ACLP mouse model, it is presently unclear whether the observed abnormal neuromuscular development of the EI is associated with the common complications seen in human GS (*i.e.* intestinal length shortening, malabsorption, growth restriction, etc). Also, babies born with GS will eventually tolerate feeding over variable periods. It has been hypothesized that once the intestine is no longer exposed to AF; normal development and maturation of intestine will resume (29). Unfortunately, the ACLP mouse model does not allow verification of this hypothesis, as affected fetuses do not survive after birth. Nonetheless, the current data provide an anatomical basis for the motility disorders observed in GS. Moreover, we feel that the overall findings from our study point toward a synergic effect of each abnormality in causing the observed GI dysmotility in GS. A decrease in ICC impairs pacemaker activity, whereas an abnormal development of enteric neurons reduces the stimuli to the SMC, which are therefore immature and are unable to develop a coordinated intestinal contractility pattern.

In summary, we described the gross morphologic and histopathological features of a recently developed genetic mouse model that exhibits an AWD that appears to be similar to human GS. Our initial histomorphological analysis suggests that intraamniotic exposure of the fetal intestine impacts on the neuromuscular development that is restricted to the EI. The ACLP mouse model appears an appropriate model for further investigations of the neuromuscular development of the EI in GS and may represent a model for developing and screening prenatal therapeutic strategies.

REFERENCES

1. Badillo AT, Hedrick HL, Wilson RD, Danzer E, Bebbington MW, Johnson MP, Liechty KW, Flake AW, Adzick NS 2008 Prenatal ultrasonographic gastrointestinal abnormalities in fetuses with gastroschisis do not correlate with postnatal outcomes. J Pediatr Surg 43:647–653
2. Eggink BH, Richardson CJ, Malloy MH, Angel CA 2006 Outcome of gastroschisis: a 20-year case review of infants with gastroschisis born in Galveston, Texas. J Pediatr Surg 41:1103–1108
3. Correia-Pinto J, Tavares ML, Baptista MJ, Estevao-Costa J, Flake AW, Leite-Moreira AF 2001 A new fetal rat model of gastroschisis: development and early characterization. J Pediatr Surg 36:213–216
4. Langer JC, Longaker MT, Crombleholme TM, Bond SJ, Finkbeiner WE, Rudolph CA, Verrier ED, Harrison MR 1989 Etiology of intestinal damage in gastroschisis. I: Effects of amniotic fluid exposure and bowel constriction in a fetal lamb model. J Pediatr Surg 24:992–997
5. Brewer S, Williams T 2004 Loss of AP-2alpha impacts multiple aspects of ventral body wall development and closure. Dev Biol 267:399–417
6. Manley NR, Barrow JR, Zhang T, Capecchi MR 2001 Hoxb2 and hoxb4 act together to specify ventral body wall formation. Dev Biol 237:130–144
7. Qu S, Niswender KD, Ji Q, van der Meer R, Keeney D, Magnuson MA, Wisdom R 1997 Polydactyly and ectopic ZPA formation in Alx-4 mutant mice. Development 124:3999–4008
8. Suzuki N, Labosky PA, Furuta Y, Hargett L, Dunn R, Fogo AB, Takahara K, Peters DM, Greenspan DS, Hogan BL 1996 Failure of ventral body wall closure in mouse embryos lacking a procollagen C-proteinase encoded by Bmp1, a mammalian gene related to Drosophila tolloid. Development 122:3587–3595
9. Layne MD, Yet SF, Maemura K, Hsieh CM, Bernfield M, Perrella MA, Lee ME 2001 Impaired abdominal wall development and deficient wound healing in mice lacking aortic carboxypeptidase-like protein. Mol Cell Biol 21:5256–5261
10. Ith B, Wei J, Yet SF, Perrella MA, Layne MD 2005 Aortic carboxypeptidase-like protein is expressed in collagen-rich tissues during mouse embryonic development. Gene Expr Patterns 5:533–537
11. Danzer E, Kiddoo DA, Redden RA, Robinson L, Radu A, Zderic SA, Doolin EJ, Adzick NS, Flake AW 2007 Structural and functional characterization of bladder smooth muscle in fetal rats with retinoic acid-induced myelomeningocele. Am J Physiol Renal Physiol 292:F197–F206
12. Stehr W, Bernal NP, Erwin CR, Bernabe KQ, Guo J, Warner BW 2006 Roles for p21waf1/cip1 and p27kip1 during the adaptation response to massive intestinal resection. Am J Physiol Gastrointest Liver Physiol 290:G933–G941
13. Hagger R, Gharaie S, Finlayson C, Kumar D 1998 Regional and transmural density of interstitial cells of Cajal in human colon and rectum. Am J Physiol 275:G1309–G1316
14. Phillips RJ, Hargrave SL, Rhodes BS, Zopf DA, Powley TL 2004 Quantification of neurons in the myenteric plexus: an evaluation of putative pan-neuronal markers. J Neurosci Methods 133:99–107
15. Hillebrandt S, Matern S, Lammert F 2003 Mouse models for genetic dissection of polygenic gastrointestinal diseases. Eur J Clin Invest 33:155–160
16. Deans KJ, Mooney DP, Meyer MM, Shorter NA 1999 Prolonged intestinal exposure to amniotic fluid does not result in peel formation in gastroschisis. J Pediatr Surg 34:975–976
17. Tibboel D, Kluck P, Molenaar JC, Gaillard JL 1987 A comparative investigation of the bowel wall in gastroschisis and omphalocele: relation to postoperative complications. Pediatr Pathol 7:277–285
18. Tibboel D, Vermey-Keers C, Kluck P, Gaillard JL, Koppenberg J, Molenaar JC 1986 The natural history of gastroschisis during fetal life: development of the fibrous coating on the bowel loops. Teratology 33:267–272
19. Wallace AS, Burns AJ 2005 Development of the enteric nervous system, smooth muscle and interstitial cells of Cajal in the human gastrointestinal tract. Cell Tissue Res 319:367–382

20. Midrio P, Faussone-Pellegrini MS, Vannucchi MG, Flake AW 2004 Gastroschisis in the rat model is associated with a delayed maturation of intestinal pacemaker cells and smooth muscle cells. J Pediatr Surg 39:1541–1547
21. Song G, David G, Hirst S, Sanders KM, Ward SM 2005 Regional variation in ICC distribution, pacemaking activity and neural responses in the longitudinal muscle of the murine stomach. J Physiol 564:523–540
22. Sanders KM, Ordog T, Koh SD, Torihashi S, Ward SM 1999 Development and plasticity of interstitial cells of Cajal. Neurogastroenterol Motil 11:311–338
23. Fu M, Chi Hang Lui V, Har Sham M, Nga Yin Cheung A, Kwong Hang Tam P 2003 HOXB5 expression is spatially and temporarily regulated in human embryonic gut during neural crest cell colonization and differentiation of enteric neuroblasts. Dev Dyn 228:1–10
24. Faussone-Pellegrini MS, Matini P, DeFelici M 1999 The cytoskeleton of the myenteric neurons during murine embryonic life. Anat Embryol (Berl) 199:459–469
25. Wiedenmann B, Franke WW 1985 Identification and localization of synaptophysin, an integral membrane glycoprotein of Mr 38,000 characteristic of presynaptic vesicles. Cell 41:1017–1028
26. Young HM, Bergner AJ, Muller T 2003 Acquisition of neuronal and glial markers by neural crest-derived cells in the mouse intestine. J Comp Neurol 456:1–11
27. Vannucchi MG, Midrio P, Flake AW, Faussone-Pellegrini MS 2003 Neuronal differentiation and myenteric plexus organization are delayed in gastroschisis: an immunohistochemical study in a rat model. Neurosci Lett 339:77–81
28. Vannucchi MG, Midrio P, Zardo C, Faussone-Pellegrini MS 2004 Neurofilament formation and synaptic activity are delayed in the myenteric neurons of the rat fetus with gastroschisis. Neurosci Lett 364:81–85
29. Midrio P, Vannucchi MG, Pieri L, Alaggio R, Faussone-Pellegrini MS 2008 Delayed development of interstitial cells of Cajal in the ileum of a human case of gastroschisis. J Cell Mol Med 12:471–478